MODIS Land Data Storage, Gridding, and Compositing Methodology: Level 2 Grid

Robert E. Wolfe, David P. Roy, and Eric Vermote, *Member, IEEE*

***Abstract*— The methodology used to store a number of the Moderate Resolution Imaging Spectroradiometer (MODIS) land products is described. The approach has several scientific and data processing advantages over conventional approaches used to store remotely sensed data sets and may be applied to any remote-sensing data set in which the observations are geolocated to subpixel accuracy. The methodology will enable new algorithms to be more accurately developed because important information about the intersection between the sensor observations and the output grid cells are preserved. The methodology will satisfy the very different needs of the MODIS land product generation algorithms, allow sophisticated users to develop their own application-specific MODIS land data sets, and enable efficient processing and reprocessing of MODIS land products. A generic MODIS land gridding and compositing algorithm that takes advantage of the data storage structure and enables the exploitation of multiple observations of the surface more fully than conventional approaches is described. The algorithms are illustrated with simulated MODIS data, and the practical considerations of increased data storage are discussed.**

I. Introduction

THE FUNCTIONAL design of satellite data production systems is based upon the processing of raw instrument data into a hierarchy of increasingly refined data products. These production processes discard large amounts of data throughout the processing chain. This forces the user community to use data that may be inappropriate for their application requirements, precludes opportunities for sophisticated users to take advantage of the entire sensed data set, and makes data reprocessing and on-demand data processing resource intensive. As new remote-sensing systems with improved geometric and radiometric quality and improved calibration stability become available, the requirement for data storage structures that will support flexible application-specific uses of the sensed data will increase. This paper describes the data storage methodology developed for terrestrial data sensed by the Moderate Resolution Imaging Spectroradiometer (MODIS).

MODIS is planned for launch onboard the morning (AM1) and afternoon (PM1) Earth Observing System (EOS) platforms in 1998 and 2000, respectively [1]. MODIS will sense all of the earth's surface in 36 spectral bands spanning the visible (0.415 μm) to infrared (14.235 μm) spectrum at nadir spatial resolutions of 1 km, 500, and 250 m. MODIS will provide both day and night full earth coverage every two days and full coverage every day for latitudes above approximately 30°. MODIS will be the primary EOS sensor for providing data on global biospheric dynamics and will reduce reliance upon data sensed by instruments such as the Advanced Very High Resolution Radiometer (AVHRR). The MODIS land science team is currently developing remote-sensing algorithms for deriving global time-series data products on various terrestrial geophysical parameters that will be used by the earth science community [2], [3]. The products include land surface reflectance, land surface temperature, spectral vegetation indexes, snow and sea ice cover, fire detection, land cover and land cover change, spectral albedo, bidirectional reflectance characterization, and a number of biophysical variables that will contribute to an improved understanding of global carbon cycles, hydrologic balances, and biogeochemical cycles.

The MODIS land data storage methodology was developed to satisfy the diverse needs of the MODIS land product generation algorithms. The requirements of the methodology are to enable efficient processing and reprocessing of MODIS land products, support flexible subsequent application of the data, provide users with all of the original, sensed MODIS observations and their subpixel geolocation information, and support the development of better science using MODIS land data. Constraining these is the requirement that the methodology does not prohibitively increase data storage costs and that mechanisms are in place to accommodate evolving data storage resources.

The MODIS land data storage methodology stores daily information concerning the MODIS observations of each part of the earth's surface. Rather than discard multiple observations of the same location, pointers to all observations that fall over a significant portion of each output geolocated grid cell are stored along with information concerning the observation/grid cell intersection. The data storage methodology will allow sophisticated users to develop their own application-specific MODIS land data sets and enable new and some existing

Manuscript received November 11, 1997; revised March 9, 1998. This work was supported under NASA Contract 9201208.

R. E. Wolfe is with Raytheon STX, NASA's Goddard Space Flight Center, Code 922, Greenbelt, MD 20771 USA (e-mail: rwolfe@kratmos.gsfc.nasa.gov).

D. P. Roy is with the Department of Geography, University of Maryland, College Park, MD 20742 USA, and NASA's Goddard Space Flight Center, Code 922, Greenbelt, MD 20771 USA.

E. Vermote is with the Department of Geography, University of Maryland, College Park, MD 20742 USA and NASA's Goddard Space Flight Center, Code 923, Greenbelt, MD 20771 USA.

Publisher Item Identifier S 0196-2892(98)04750-0.

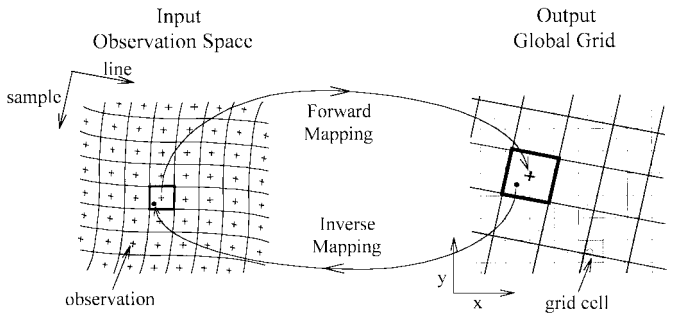

Fig. 1. Gridding process and examples of forward and inverse mapping between the input-sensed observation space (left) and the output geometrically correct space (right).

remote-sensing algorithms to be more accurately developed. A generic MODIS land gridding and compositing algorithm that takes advantage of the data storage structure is described to illustrate these points.

II. Conventional Storage of Global Satellite Remotely Sensed Data: Gridded and Composited Data

Commonly only raw and highly processed, global satellite, remotely sensed data sets are archived and distributed to the user community. The processed data sets are typically geometrically corrected data that have been mosaicked and temporally composited into a single representation of the surface. The geometric correction process reconstructs remotely sensed data into a new image grid with known earth-based coordinates that may be navigated like a map. Satellite data must be geometrically corrected to remove geometric distortions caused by the instrument viewing geometry, the curvature of the earth, surface relief, and perturbations in the motion of the instrument relative to the surface. Geometric correction can be considered a two-stage process. First, the sensed image observations are geolocated, and then secondly, the geolocated observations are gridded into an output grid. Different orbits of geometrically corrected satellite data may then be combined using a compositing routine. Composited data are assumed to be representative of the surface over the compositing period and to have reduced cloud and atmospheric contamination [4]. The gridding and compositing procedures and some terminology used in the rest of this paper are described below.

A. Gridding

The allocation of geolocated image observations into an output image grid is termed gridding and is illustrated in Fig. 1. The pixels defined by the output image grid will be referred to as grid cells. The left half of Fig. 1 illustrates the input observation space viewed by the instrument and shows the dimensions and location of each sensor observation on the earth's surface. In practice, the observations will have elliptical shapes as the surface area convolved with the system point spread function (PSF) defines the area that is physically sensed [5]. The right half of Fig. 1 illustrates how these observations may fall relative to a geometrically correct output image grid. The grid cell coordinates are predefined by specifying the grid cell dimensions and the origin and orientation of the output grid in some earth-based coordinate system. The observations and grid cells have different dimensions and are misaligned.

There are generally two gridding approaches: a forward mapping approach, in which the observations are mapped into the output grid, and an inverse approach, in which the grid cells are mapped into the sensed image (Fig. 1). Both approaches will introduce artifacts or change the structure of the output gridded image where the grid cells and observations do not match exactly.

In the forward gridding approach, sometimes known as the direct method [6] or pixel carryover [7], each observation is allocated to the grid cell that the observation center falls within. When two or more observations map into the same grid cell, a decision is made as to which observation to keep; usually, the observation falling closest to the grid cell center is selected. The forward gridding approach is computationally inefficient as grid cells may be addressed more than once.

In the inverse gridding approach, sometimes known as the indirect method [6] or pixel filling [7], each grid cell center is mapped into the sensed image. The grid cell value is then interpolated from a local neighborhood of surrounding observations. The interpolation process is known as image resampling. Nearest-neighbor resampling is the simplest resampling method and works by allocating the value of the nearest observation to the grid cell. More sophisticated resampling functions were developed to approximate the theoretically optimal sinc resampling function, which cannot be implemented, as it requires an infinitely large pixel neighborhood [8]. These functions include bilinear, cubic convolution, and truncated sinc resamplers [8]–[10].

The forward gridding approach and the nearest-neighbor resampling approach produce the same result. Both are commonly used because they are computationally simple and do not alter the values of the original sensed data. They may, however, introduce subpixel geometric discontinuities (up to a maximum of $\sqrt{2}/2$ of an observation dimension) and discard observations completely. The more complex, inverse-gridding, resampling methods alter the radiometric values of the original sensed data [9]–[11].

None of the gridding approaches consider the degree of overlap of different observations that may fall within each grid cell. The forward gridding and the nearest-neighbor resampling methods select only a single observation per grid cell. The other resampling methods assume that the observations are distributed evenly across the earth's surface. However wide field-of-view, whiskbroom sensors, such as the AVHRR [5], [12] and MODIS [1], [13], have progressively overlapping observations further from nadir. Image-restoration-based approaches that use knowledge of the system PSF and the observation/grid cell intersection geometry have been suggested [14], [15]. Restoration techniques have not been implemented operationally because of difficulties reliably defining the system PSF (the convolution of the dynamic instrument PSF with a variable atmospheric PSF) and because they are susceptible to image noise [15].

B. Compositing

Compositing procedures are applied to time series of geometrically correct image data in an attempt to produce a single representative data set. They are typically applied to multiple orbits of data sensed within the same day and orbits of data sensed over a period of several days to a month. They either select the "best" observation of a grid cell based on some criteria or combine multiple observations of the same grid cell. Compositing criteria have included the maximum normalized difference vegetation index (NDVI), maximum brightness temperature, maximum surface temperature, maximum difference in red and near-infrared reflectance, minimum scan angle, maximum thermal radiance, and combinations of these [4], [16]–[19]. The criteria are designed to ideally select from the time series only near-nadir observations that have reduced cloud and atmospheric contamination. However, some of these criteria have been shown to select AVHRR observations due to bidirectional reflectance effects rather than reduced atmospheric or cloud contamination [17], [20]. Compositing algorithms that model the bidirectional reflectance have been developed to compensate for this problem and combine all or most of the observations of the grid cell [21]. The reliance of compositing procedures upon geometrically correct data may introduce biases caused by registration errors and by changes in the effective spatial resolution of the data across the image swath.

Registration errors between colocated grid cells sensed in different orbits will interact with the compositing criteria to introduce compositing biases over heterogeneous scenes. For example, AVHRR time series are commonly composited using the maximum NDVI. Gridding and geolocation errors found between colocated grid cells may lead to the preferential selection of vegetated grid cells (high NDVI) over nonvegetated grid cells (low NDVI) found in different orbits. This may enlarge the boundaries of vegetation features, cause small isolated nonvegetated features to shrink or disappear, and smooth heterogeneous vegetated/nonvegetated scenes.

Typically, the grid cell dimensions are set equal to the nadir observation dimensions. As a result, geometrically corrected wide field-of-view data contain similar or replicated pixel values toward the edges of the sensed image swath, where the observation dimensions are greater than the grid cell dimensions. Conventional compositing procedures, such as the maximum NDVI, select gridded observations without consideration of their viewing geometry, although a view zenith threshold is often used to remove observations sensed at high-view zenith angles. Gridded observations sensed in one orbit with high-view zenith angles may be selected rather than near-nadir gridded observations sensed in a different orbit. Over heterogeneous scenes, this causes a reduction in the effective spatial resolution of the composited data.

III. MODIS Instrument

A. MODIS Sensing Geometry

MODIS will orbit the earth on the EOS-AM1 platform at an altitude of 705 km in a near-polar orbit, with an inclination of 98.2° and a mean period of 98.9 min. MODIS has a field-of-view of 110° and will sense all of the equator every two days. Full coverage of the globe will occur daily above approximately 30° latitude, where different orbit swaths overlap in the across-track direction as the orbits converge polewards.

MODIS will acquire earth observations in 36 spectral bands: 29 with 1-km (at nadir) pixel dimensions, five with 500-m pixels, and two with 250-m pixels. Each scan line of MODIS data is composed of 1354 1-km, 2708 500-m, and 5416 250-m observations. The scan lines are elongated because of the curvature of the earth such that the MODIS swath width is approximately 2340 km. The instrument's integration time matches the data sampling rate so that the 500-m bands are offset in the along-scan direction by 250 m at nadir relative to the 1-km bands and the 250-m bands are offset by 125 m relative to the 500-m bands [13]. MODIS is a whiskbroom sensor that simultaneously senses ten rows of 1-km detector pixels, 20 rows of 500-m detector pixels, and 40 rows of 250-m detector pixels as the scan mirror sweeps across track. Fig. 2(a) illustrates the along- and across-track dimensions of the MODIS 1-km observation footprint as a function of view zenith angle. Fig. 2(b) illustrates the typical coverage of three consecutive scans on the earth's surface. The whiskbroom configuration and the forward velocity of the satellite are configured such that the leading edge of one scan will start to overlap the trailing edge of the next scan (10% overlap) at scan angles greater than 24° from nadir. This overlap increases until at the scan edge there is almost 50% overlap [Fig. 2(b)]. This effect is referred to as the "bowtie" effect and is present in AVHRR data as well as MODIS data [5].

B. MODIS Geolocation Accuracy

MODIS land applications require subpixel geolocation accuracy to support change detection and accurate retrieval of biophysical parameters over heterogeneous surfaces [22]. MODIS geolocation is performed using onboard measurements of the sensor attitude and position combined with models of the sensing geometry and the earth to geolocate each 1-km observation [13]. Terrain effects are modeled using a global digital terrain model defined with a spatial resolution of 1 km [23]. The 500-m and 250-m MODIS observations are geolocated using a fixed offset relative to the 1-km observations. The geolocation coordinates are defined in latitude and longitude in the WGS84 geodetic system [24]. The MODIS geolocation design specification is 0.15 of a 1-km observation (1σ) with an operational goal of 0.05 of a 1-km observation (1σ) to be achieved after postprocessing using ground control points [25]. The operational geolocation goal of 0.05 of a 1-km band observation corresponds to 5, 10, and 20% of a 1-km, 500-m, and 250-m MODIS nadir observation, respectively.

C. MODIS Product Terminology

Raw MODIS instrument data are processed into a hierarchy of increasingly refined data product levels that are summarized in Table I. Raw MODIS data (Level 0) are calibrated and geolocated (Level 1), then converted into some geophys-

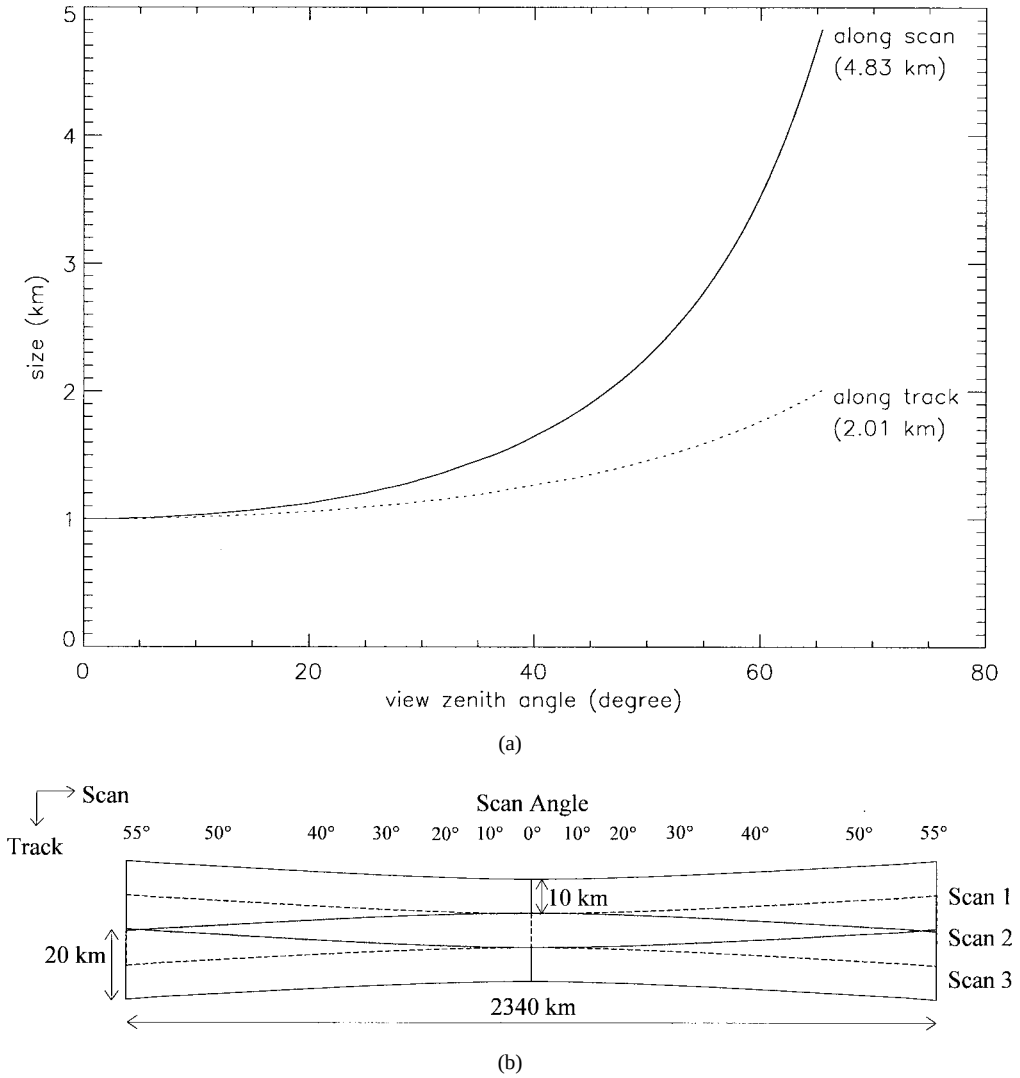

Fig. 2. MODIS sensing geometry: (a) along- and across-track dimensions of the MODIS 1-km observation footprint as a function of view zenith angle and (b) three consecutive MODIS scans showing the "bowtie" effect (scan 2 is shown shaded).

TABLE I
MODIS DATA PRODUCT LEVEL HIERARCHY

Level 0	Raw MODIS data at original resolution, time order-restored.
Level 1	Level 0 observations to which radiometric calibration algorithms have been applied to produce radiances or irradiances at the original MODIS resolution. Geolocation data, calibration data and other ancillary data are stored.
Level 2	Geophysical parameter data retrieved from the Level 1 data by application of geophysical parameter algorithms. Retrieved data are at the same location and resolution as the Level 1 data.
Level 3	Geometrically corrected Level 2 data, which have been gridded and may have been temporally composited. The data are defined in a known earth based coordinate system.

ical parameter of interest (Level 2), and finally, gridded and/or composited into some earth-based coordinate system (Level 3). MODIS land product algorithms are used to produce Level 2 and Level 3 products.

The smallest amount of MODIS land data that is stored is defined at Levels 1 and 2 as a granule and at Level 3 as a tile. The granules and tiles are defined separately for different resolutions. A granule corresponds to approximately 5 min of MODIS observations and covers approximately 2340 × 2000 km. The Level 3 data products are gridded and stored as fixed, nonoverlapping, earth-located tiles rather than granules. Each tile has an area of approximately 1200 × 1200 km (10 ×10° at the equator) and may be defined in Integerized Sinusoidal, Goode Homolosine, and Lambert Azimuthal Equal-Area map projections [26]. The tiles are illustrated in Fig. 3. Globally, there are 326 tiles that contain land.

IV. NEW METHOD FOR STORAGE OF GLOBAL REMOTELY SENSED DATA: MODIS LAND LEVEL 2 GRID

The MODIS land data storage approach is developed to preserve as much information as possible about each observation of a grid cell. The approach is purposefully general to accommodate the multiplicity of MODIS land products that are being developed and to facilitate future development of terrestrial remote-sensing algorithms. It may be adapted to

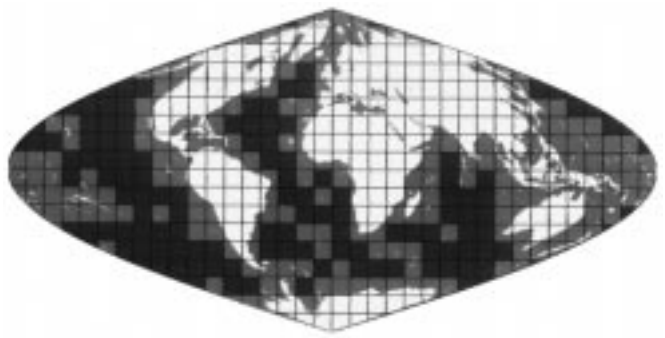

Fig. 3. MODIS land Level 3 tile structure (shown in the Integerized Sinusoidal map projection).

store any remotely sensed data set that can be geolocated to subpixel accuracy. The approach will be used to store MODIS land gridded products defined at 1 km, 500 m, and 250 m.

A. Approach

The MODIS land data storage approach is called Level 2 Grid (L2G). The L2G structure stores information concerning the Level 2 observations that fall within each Level 3 grid cell over a 24-h (GMT) period. The multiple observations stored in the L2G structure may be examined by a Level 3 process to extract only the most relevant observations falling over each grid cell. In this way, multiple observations intersecting or overlapping the same grid cell are kept for input to the Level 3 process, which may then be implemented in a more accurate and robust manner.

The logical structure of the L2G storage approach is illustrated in Fig. 4. Each L2G product has the same spatial dimensions and contains the same number of rows and columns of grid cells as its corresponding Level 3 tile. Three types of data are stored for each observation per L2G grid cell: pointer information, Level 2 geophysical parameter(s), and sensing geometry information. The multiple observations that fall over each grid cell are ranked, and their L2G data are stored so that the observation that covers most of the grid cell is stored first and the observation that covers the grid cell the least is stored last. The ranking is for visualization convenience and has no impact on the subsequent use of the data. Each data type is stored as a separate L2G product to ensure efficiencies in data storage, data access, and data reprocessing. The three data types are described below.

1) L2G Pointer: In computer science, a pointer is defined as a variable that holds a memory address. Similarly, the L2G pointer stores the addresses of the L2 observations that intersect each L2G grid cell. Information concerning the observation and grid cell intersection are also stored. Table II summarizes the stored information.

Granule pointer, *line*, and *sample* define the Level 2 granule and the location of the observation within the granule. $\Delta line$ and $\Delta sample$ describe the location of the observation center relative to the grid cell center as a fraction of the observation line and sample dimensions (Fig. 5). $\Delta line$ and $\Delta sample$ may be used to implement subgrid cell accuracy Level 3 processes. The observation center may fall outside of the grid cell if the

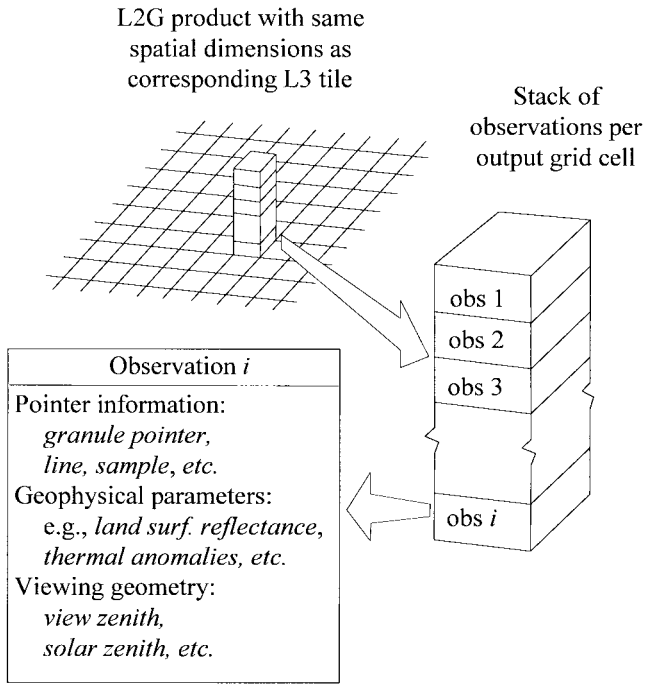

Fig. 4. Logical structure of the Level 2 Grid data storage approach.

TABLE II
POINTER INFORMATION STORED IN THE L2G POINTER PRODUCT FOR EACH GRID CELL

Name	Description
granule pointer	Pointer to a unique granule ID
line	Scan line number of the observation in the Level 2 granule
sample	Sample number of the observation in the Level 2 granule
$\Delta line$	Sub-pixel scan line offset (1/64 nadir observation dimension precision)
$\Delta sample$	Sub-pixel sample offset (1/64 nadir observation dimension precision)
obscov	Observation coverage percentage (ratio of the observation/grid cell intersection area to the observation area)
Additional Fields Stored Only at 500 m and 250 m	
obsptr	Pointer to corresponding observation at next coarse resolution
rowres, colres	Row and column location residuals (for locating the corresponding observation at next coarse resolution)

observation is larger than the grid cell, but it may still be stored dependent upon the relative observation/grid cell intersection [this is discussed in Section V(b)]. MODIS land L2G products are gridded with the grid cell dimension set equal to the nadir observation dimension so that the grid cell is never larger than the observation.

Obscov defines the observation/grid cell intersection area divided by the area of the observation footprint. The observation footprint is the surface area sensed by each instantaneous field-of-view and is computed using simple or complex models that can be switched in production according to processing load constraints. The simple observation footprint is modeled as a convex four-sided polygon with corner locations calculated by bilinear interpolation of the neighboring geolocated

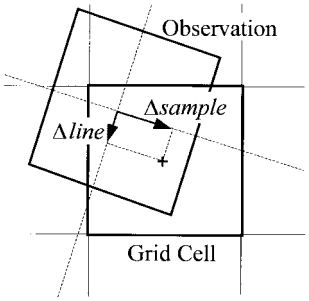

Fig. 5. Definition of the location of a grid cell center within an observation (observation shown shaded).

observation centers. The complex model takes into account the MODIS PSF and across-track scan rate. Because MODIS scans at a rapid rate in the across-track direction, the PSF is modeled as a square area integrated over the entire sampling interval, giving a triangular PSF across track and a square PSF along track. The grid cell area is predefined by the Level 3 tile geometry. The observation and grid cell intersection area is derived using efficient polygon intersection algorithms [27]. *Obscov* may be used by Level 3 processes to rank the relative contributions of each observation to a given grid cell.

Obsptr, *rowres*, and *colres* are stored in the 250-m and the 500-m L2G pointer products to enable navigation between the different MODIS spatial resolutions. The 250-m and the 500-m data are used to map the 250-m and the 500-m observations to the 500-m and the 1-km observations, respectively.

2) L2G Geophysical Parameter: The Level 2 geophysical parameters (e.g., surface reflectance, thermal anomalies, and snow and sea ice) and ancillary quality assurance information are stored for each observation that is referenced in the corresponding L2G pointer product.

3) L2G Sensing Geometry: The viewing geometry (sensor view zenith and azimuth angles), the slant range (distance from the sensor to the surface), and the solar geometry (solar zenith and azimuth angles) are stored for each 1-km observation that is referenced in the 1-km L2G pointer product. These data are required for implementation of most of the MODIS land Level 3 product generation algorithms. Users requiring sensing geometry information at 500 or 250 m may use obsptr, rowres, and colres to find the corresponding 1-km observation and then interpolate the information as required.

B. L2G Production

The L2G products are produced at the end of each day (24-h period) when the Level 2 products for that day have been generated. L2G products that only use daytime data will only store observations sensed during the daylight portion of each orbit. Fig. 6 illustrates the procedure used to compute the L2G products. The procedure is performed on a tile-by-tile basis.

The process is started by establishing which Level 2 granules produced over the 24-h period intersect each Level 3 tile. This is performed for each tile by geometric intersection of the predefined tile boundary with the day's Level 1 geolocation granules that define the positions of each observation. The comparison is performed in latitude and longitude coordinates.

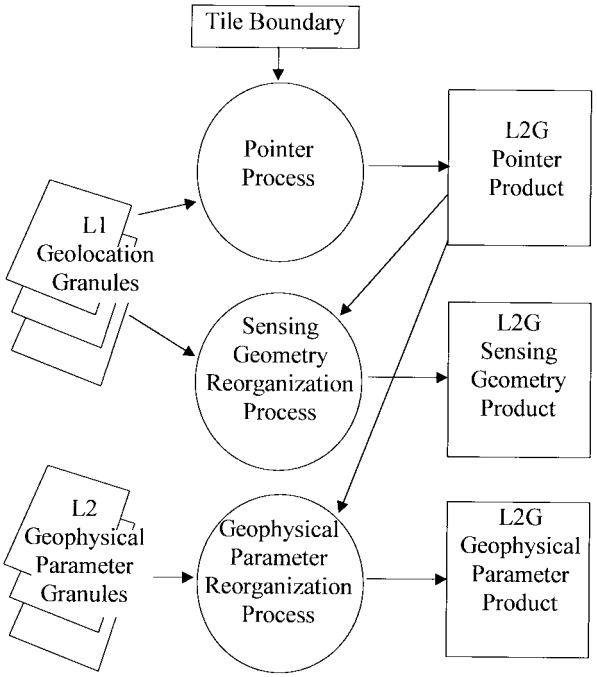

Fig. 6. Production of the Level 2 Grid Pointer, Sensing Geometry, and Geophysical Parameter products. Processing performed on a tile-by-tile basis (see text for explanation).

All observations that fall within the Level 3 tile are then projected into the required Level 3 map projection.

The pointer process first computes which observations are stored for each Level 3 grid cell. To reduce the L2G storage volume, the ratio of the observation/grid cell intersection to the grid cell area *(cellcov)* is computed and used to discard observations that cover less than a prespecified portion of each grid cell. The L2G pointer and supplementary geometric information (Table II) are calculated for the remaining observations and written to an L2G pointer product.

The L2G pointer product is examined by a sensing geometry and geophysical parameter reorganization process to produce a corresponding L2G sensing geometry and L2G geophysical parameter product. The sensing geometry reorganization process reads the Level 1 geolocation granules to pick up the required 1-km sensing geometry information. The geophysical parameter reorganization process reads the Level 2 geophysical parameter granules to pick up the required Level 2 geophysical parameter(s). These processes are performed for each observation stored in each grid cell referenced in the L2G pointer product.

The L2G production procedure saves significant computational resources for generation of the MODIS Level 3 land products and for on-demand processing and for reprocessing of these products. The procedure is performed once instead of separately for each Level 3 process. For example, all Level 3 processes that require gridded land surface reflectance data read the same L2G land surface reflectance products and do not need to independently locate, combine, intersect, and geometrically correct individual Level 2 land surface reflectance granules. If the geophysical parameters need to be reprocessed, unless the geolocation data have changed,

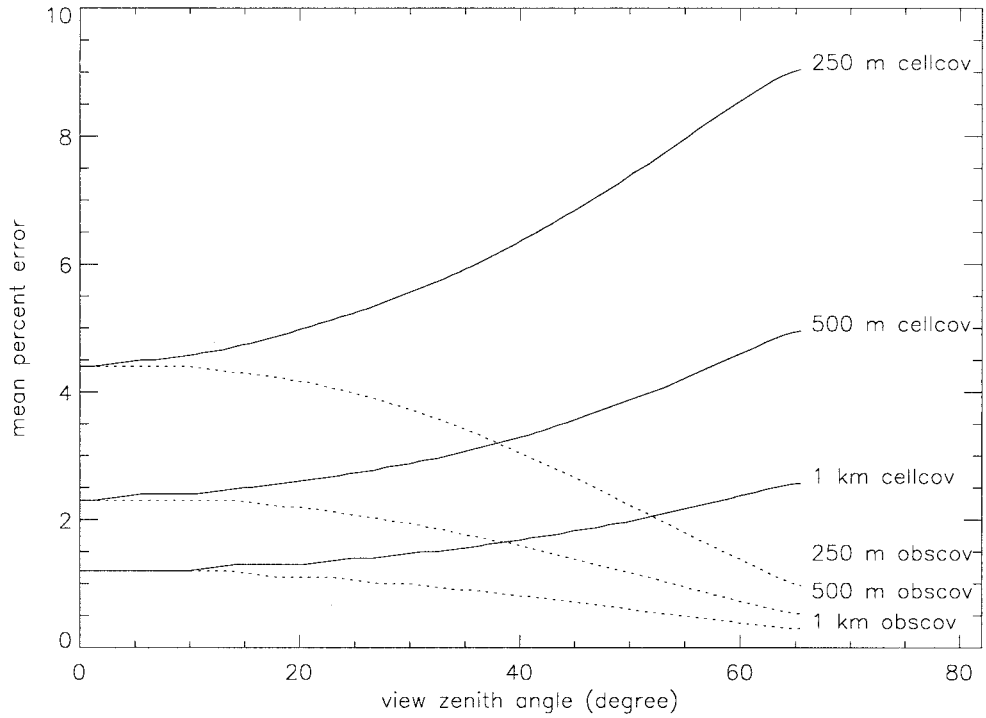

Fig. 7. Mean percent error in *obscov* and *cellcov*, with respect to MODIS view zenith angle, given the MODIS 1σ geolocation error equivalent to 0.05 of a 1-km observation. Errors shown for MODIS 1-km, 500-m, and 250-m MODIS bands.

only the Level 2 geophysical parameter granules need to be reprocessed, as the L2G pointer products remain unchanged.

V. MODIS L2G Considerations

This section discusses some specific aspects of the L2G approach, with respect to sensitivity to the MODIS geolocation accuracy and data storage volume. The L2G approach is then compared with a more conventional approach of storing individual orbits of nearest-neighbor resampled data.

A. Geolocation Accuracy

The L2G approach can only be meaningfully implemented if the observations are geolocated to subpixel accuracy. If the MODIS geolocation accuracy is only as good as the design specification (0.15 of a 1-km observation 1σ) and not the operational goal (0.05 of a 1-km observation 1σ), the L2G approach may not be suitable for storage of the 500-m bands and will not be suitable for storage of the 250-m bands. This is because the design specification geolocation accuracy may result in geolocation errors that are larger than the 250-m observation dimension and larger than half the 500-m observation dimension. Subpixel geolocation errors will be propagated in a directly proportional manner into the L2G subpixel data $(\Delta line, \Delta sample)$. They may also affect which observations are stored in each grid cell. This latter issue is not a problem for the storage of single orbits of MODIS data. This is because relative geolocation errors between adjacent observations and between consecutive scan lines can be assumed to be negligible (high-temporal frequency attitude perturbations are damped by stabilization of the sensor platform, and surface relief distortions are likely to be correlated between neighboring observations). Consequently, adjacent observations sensed in the same orbit will be stored in the same or adjacent grid cells regardless of the subpixel geolocation accuracy. However, this may not be the case for observations falling over the same grid cell but sensed by different satellite overpasses. This is because the geolocation errors in whiskbroom sensor data are a function of the viewing geometry and of time-varying errors in the sensor position and attitude [28].

A sensitivity analysis was performed to examine the impact of MODIS geolocation errors upon *obscov* and *cellcov*. *Obscov* defines the ratio of the observation/grid cell intersection to the observation area and is of importance to the L2G user, as it may be used to rank the relative contributions of the observations that fall in each grid cell. *Cellcov* defines the ratio of the observation/grid cell intersection to the grid cell area and is used to determine which observations are stored for each L2G grid cell.

Fig. 7 illustrates the mean percentage error in *obscov* and *cellcov*, with respect to the MODIS viewing geometry, given the MODIS 1σ geolocation error of 0.05 of a 1-km observation. The errors are shown for the 1-km, 500-m, and 250-m MODIS bands. The errors were computed using the simple observation footprint model (convex four-sided polygon) with the observation dimensions scaled according to the view zenith angle [Fig. 2(a)]. The orientation of the grid cells and the observation footprints at 1 km, 500 m, and 250 m were considered to be in perfect alignment. For each view zenith angle, the grid cell was translated across the observation in steps of one hundredth of the observation x and y dimensions.

TABLE III
MEAN, MINIMUM, AND MAXIMUM OF THE MEAN PERCENTAGE ERRORS IN *obscov* AND *cellcov* OVER THE MODIS FIELD-OF-VIEW FOR MODIS 1-km, 500-m, AND 250-m BANDS, GIVEN THE MODIS 1σ (0.05 OF A 1-km OBSERVATION) AND 2σ (0.1 OF A 1-km OBSERVATION) GEOLOCATION ERRORS. PERCENTAGE ERRORS EXPRESSED TO ONE DECIMAL PLACE

		obscov			*cellcov*		
		1 km	500 m	250 m	1 km	500 m	250 m
1 σ error	min	0.3	0.5	0.9	1.2	2.3	4.4
	mean	0.9	1.7	3.3	1.6	3.2	6.0
	max	1.2	2.3	4.4	2.6	5.0	9.1
2 σ error	min	0.5	0.9	1.6	2.3	4.4	7.9
	mean	1.7	3.3	5.9	3.2	6.0	10.7
	max	2.3	4.4	7.9	5.0	9.1	15.6

TABLE IV
MEAN NUMBER OF OBSERVATIONS STORED PER L2G GRID CELL ACROSS A MODIS SWATH USING DIFFERENT *cellcov* THRESHOLDS. *Cellcov* DEFINES THE RATIO OF THE OBSERVATION/GRID CELL INTERSECTION TO THE GRID CELL AREA AND IS USED TO DETERMINE WHICH OBSERVATIONS ARE STORED FOR EACH L2G GRID CELL. ONLY OBSERVATIONS COVERING A GRID CELL WITH *cellcov* VALUES GREATER THAN A FIXED THRESHOLD ARE STORED. DATA EXPRESSED TO TWO DECIMAL PLACES

cellcov threshold	mean number of observations stored per grid cell over a MODIS swath
0	4.00
5	2.98
10	2.65
15	2.36
20	2.11
25	1.88
30	1.67

At each of the 10 000 positions, the grid cell coverage and the observation coverages were computed and compared to eight misaligned coverages. The misalignments were simulated by shifting the grid cell center in eight compass directions by an appropriate x, y, or diagonal component of the 0.05 of a 1-km observation geolocation error. The mean of the absolute differences between the aligned and misaligned coverage estimates over all positions were then calculated for each MODIS view zenith angle.

For all MODIS bands, the grid cell coverage *(cellcov)* errors increase and the observation coverage *(obscov)* errors decrease with increasing view zenith angle (Fig. 7). This is because the area of the observation footprint increases at greater view zenith angles, but the grid cell dimension remains fixed. The errors are greater for the higher spatial resolution bands because the geolocation error corresponds to a larger fraction of each observation. The mean, minimum, and maximum of the mean percentage errors in *obscov* and *cellcov* over the MODIS swath are summarized in Table III for MODIS 1σ and 2σ geolocation errors. Assuming that the MODIS geolocation errors are normally distributed, geolocation errors less than the 1σ error (0.05 of a 1-km observation) and less than the 2σ error (0.1 of a 1-km observation) will occur approximately 68 and 95% of the time, respectively. The maximum 2σ 250-m *obscov* error is 7.9%, and the maximum 2σ 250-m *cellcov* error is 15.6%. L2G users should consider the *obscov* errors according to their application requirements. The *cellcov* errors are of importance in considering L2G data storage volumes, which are discussed below.

B. L2G Data Storage Volume

The science requirements of the MODIS land product generation algorithms will be met without storing all MODIS observations of the earth over a 24-h period. This is achieved by discarding all observations that cover less than a certain portion of each grid cell, storing only land observations, and discarding certain MODIS land products over polar regions (above 80° latitude N and 60° latitude S) where they are not relevant.

The L2G data storage volume is primarily reduced by discarding all observations that cover less than a certain portion of each grid cell. This is implemented by only storing observations covering a grid cell with *cellcov* threshold values greater than a fixed threshold. The threshold was set by consideration of the subsequent utility of the L2G data and potential data storage savings. A 24% *cellcov* was adopted for storage of the MODIS L2G products because it is the highest threshold that can be used without completely discarding observations. In the case when an observation intersects four adjacent grid cells equally, the 24% *cellcov* threshold will ensure that the observation is not discarded from the L2G data set (but instead is stored in all four grid cells). Table IV shows the mean number of observations stored per grid cell across a MODIS swath using different *cellcov* thresholds. The data were calculated assuming a Level 3 grid lying parallel to the MODIS swath and in the same manner as the *obscov* and *cellcov* error analysis. As the *cellcov* threshold increases, the mean number of observations stored per grid cell decreases. Because of the increasing overlap between consecutive scan lines further from nadir [Fig. 2(b)], an average of four observations are stored per grid cell across the image swath if all observations are stored (0% *cellcov* threshold). Using the 24% *cellcov* threshold gives approximately two observations stored across the image swath (Table IV) and, therefore, reduces the L2G storage volume by approximately 50%.

The *cellcov* sensitivity to MODIS geolocation errors (Fig. 7, Table III) may result in the incorrect allocation of observations to grid cells. This implies a reduction in the utility of the L2G data as the $\Delta line$, $\Delta sample$, and *obscov* pointer information will be defined, with respect to the incorrect grid cell. Fig. 8 illustrates the mean percentage of observations incorrectly stored per L2G grid cell using a *cellcov* threshold of 24% and assuming MODIS 1σ and 2σ geolocation errors. The data were calculated in a similar manner as the *obscov* and *cellcov* error analysis. As before for each view zenith angle, a grid cell was translated across the observation in steps of one hundredth of the observation x and y dimensions. At each of the 10 000 positions, *cellcov* was computed and then compared with the *cellcov* values of eight misaligned observations simulated by shifting the grid cell center in eight compass

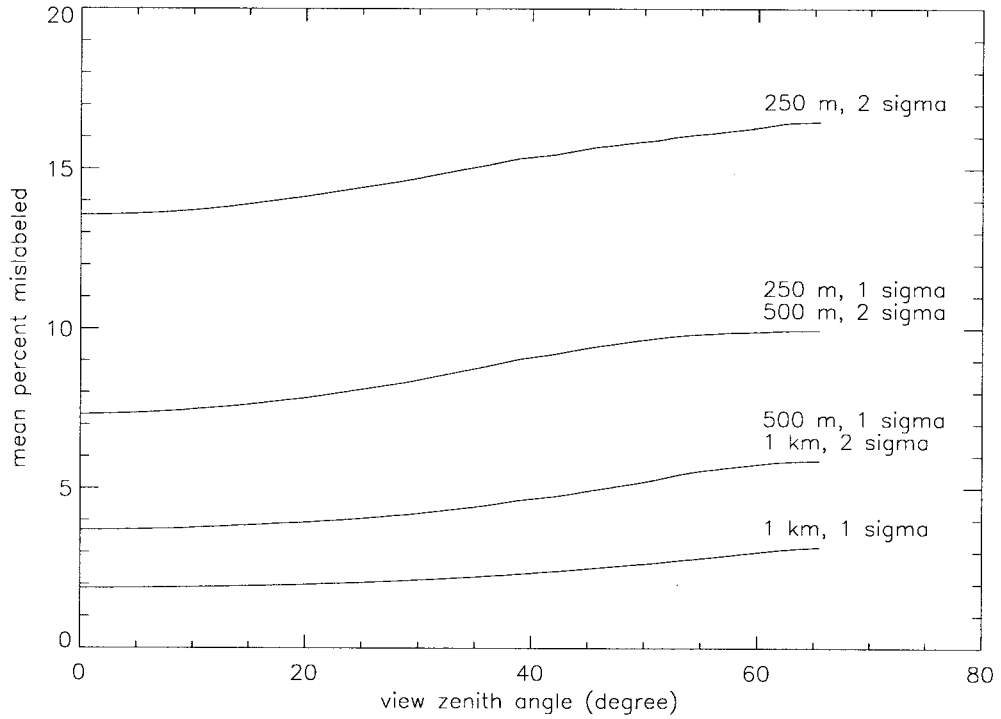

Fig. 8. Mean percentage of observations incorrectly stored per grid cell in the L2G structure, given the MODIS land *cellcov* threshold of 24%. The data are shown, with respect to the MODIS view zenith angle, given the MODIS 1σ geolocation error (equivalent to 0.05 of a 1-km observation) and given the MODIS 2σ geolocation error (equivalent to 0.1 of a 1-km observation) for MODIS 1-km, 500-m, and 250-m MODIS bands.

directions by an appropriate x, y, or diagonal component of the observation geolocation error. The misaligned observations were considered to be incorrectly omitted if their *cellcov* value was less than or equal to the 24% *cellcov* threshold, while the aligned observation *cellcov* value was greater than the threshold. The misaligned observations were considered to be incorrectly retained if their *cellcov* value was greater than the 24% *cellcov* threshold, while the aligned observation *cellcov* value was less than or equal to the threshold. The mean number of misaligned observations incorrectly stored were computed at each view zenith angle and are illustrated in Fig. 8. The mean number of observations incorrectly stored increase with increasing view zenith angle, geolocation error, and spatial resolution. Less than 3, 6, and 10% of the 1-km, 500-m, and 250-m observations, respectively, are incorrectly stored given a MODIS 1σ geolocation error. MODIS 2σ geolocation errors will occur only rarely but will cause at most 6, 10, and 16.5% of the 1-km, 500-m, and 250-m observations to be incorrectly stored, respectively. An average of approximately 15% of the 250-m observations will be incorrectly stored in the L2G data given a MODIS 2σ geolocation error.

Table V summarizes the global Level 2, L2G, and Level 3 daily data storage volumes of the MODIS land surface reflectance product. The table demonstrates the large difference between the Level 2 and L2G data storage requirements and the efficiencies made by only storing land and nonpolar regions. The L2G product requires 18 times more data storage than the Level 2 product if all observations of the globe are stored (0% *cellcov* threshold). This is because there are more grid cells than there are MODIS observations (due to the viewing geometry, constant scan rate, and earth curvature) and because of the additional pointer and supplementary geometric information stored for each observation. Discarding observations using the 24% *cellcov* threshold reduces this multiplication factor to 8.9. The L2G global storage requirements are reduced by approximately 43% by eliminating all nonland

TABLE V
GLOBAL DAILY (12 h) LAND SURFACE REFLECTANCE DATA STORAGE VOLUMES FOR LEVEL 2, LEVEL 2G* (*cellcov* THRESHOLD = 0%), LEVEL 2G (*cellcov* THRESHOLD = 24%), AND LEVEL 3 PRODUCTS. DATA STORAGE VOLUMES IN Gbytes PER DAY. (THE LEVEL 3 PRODUCT IS A SUMMARY OF EIGHT DAYS OF L2G DATA, SO THAT IT HAS AN AVERAGE DAILY VOLUME OF AN EIGHTH OF THE VOLUME SHOWN)

	Global (all Earth surface)				Global (land surface only)		Global (land without poles)	
Data Set	**L2**	**L2G***	**L2G**	**L3**	**L2G**	**L3**	**L2G**	**L3**
500 m Land Surface Reflectance (5 bands and quality assurance information)	22	164	80	37	45	26	38	23
250 m Land Surface Reflectance (2 bands and quality assurance information)	37	311	155	64	89	45	74	40
Sub-Total	59	475	235	101	134	71	112	63
1 km Observation Pointer		22	11		6		5	
500 m Observation Pointer		110	54		31		26	
250 m Observation Pointer		440	217		124		104	
1 km Sensing Geometry		17	8		5		4	
Sub-Total		589	290		166		139	
Total	59	1064	525	101	300	71	251	63

observations and are reduced again by approximately 14% by not storing polar observations.

C. Comparison of L2G Data Storage Approach with a Conventional Data Storage Approach

Conventionally individual orbits of satellite data are geometrically corrected and gridded using nearest-neighbor resampling, which does not alter the radiometry of the data. Different orbits sensed over a day may be stored separately or together as a three dimensional data structure, with two dimensions defining the spatial extent of the data and the third dimension defining the different orbits. This conventional approach does not handle the bowtie effect, precludes opportunities for users to take advantage of the unresampled data, and makes data reprocessing and on-demand data processing resource intensive. The L2G approach has several scientific advantages over the conventional approach, with respect to the subsequent utility of the data. These are illustrated in Section VI for gridding and compositing applications. In particular, the L2G approach allows the user to take advantage of the high-MODIS geolocation accuracy. The subgrid cell geometry of nearest-neighbor resampled observations will be unknown as nearest-neighbor resampling may introduce geometric discontinuities up to a maximum of $\sqrt{2}/2$ of the observation dimension. The L2G approach stores the subgrid cell geometry for each observation ($\Delta line, \Delta sample$, *obscov*). Both the conventional and the L2G approach are sensitive to geolocation errors. The maximum MODIS 2σ geolocation error will cause no more than an 8% error in *obscov* (Table III) and will be propagated in a directly proportional manner into $\Delta line$ and $\Delta sample$. For sufficiently large geolocation errors, observations may be incorrectly assigned to grid cells. This will make the L2G approach less useful than the conventional approach as the L2G sub grid cell geometric information will be redundant and stored unnecessarily. This will occur on average for approximately 15% of the L2G 250-m data, given a MODIS 2σ geolocation error.

The primary disadvantage of the L2G data storage approach is that of increased data storage. For production systems that produce many products in parallel, such as MODIS land, processing efficiencies gained by adoption of a common L2G structure will outweigh data storage costs. It is recognized, however, that this balance will not be found for the production and storage of individual products.

VI. MODIS Land Gridding and Compositing

The generic MODIS land gridding and compositing approach described in this section takes advantage of the L2G data structure and illustrates several of its benefits. L2G tiles are examined to extract only the most relevant observations falling under each output grid cell. This allows the efficient geometric gridding and compositing of remotely sensed data sets without loss of potentially important subpixel data and precludes some of the problems with conventional methods described in Section II.

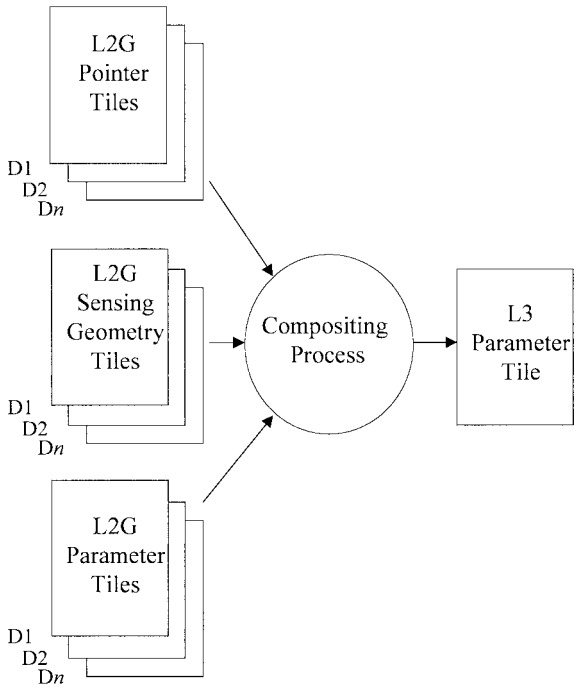

Fig. 9. Compositing a Level 3 geophysical parameter tile from n days of Level 2 data using the Level 2 Grid structure.

A. L2G Gridding Approach

The different MODIS land map projections are processed efficiently by transforming the geolocated coordinates of the MODIS observations into the required map projection and then extracting the required L2G geophysical parameters for gridding. This is advantageous, as the observations are only resampled once, avoiding unnecessary degradation of the gridded data. Similarly, a sophisticated user may define a different map projection by transforming the geolocated observation coordinates and then gridding the L2G geophysical parameters.

A Level 3 gridded product may be produced using the L2G structure from a single orbit of data or from multiple observations sensed by different orbits and resulting from the bowtie effect. Different observations of the same grid cell can be filtered to discard unwanted observations by examination of corresponding L2G sensing geometry and geophysical parameter tiles.

The L2G structure will enable new gridding techniques to be developed. Conventional resampling algorithms, such as the cubic convolution resampling function, are based upon sampling theorems that assume that the data are sampled uniformly in space [8]. The information concerning the observation/grid cell intersection and their subpixel position may be used to implement new techniques designed to compensate for the changing sampling density found in MODIS data. Such information may be used to perform image restoration. For example, restoration techniques may be applied to multiple observations of the same grid to enable the production of higher spatial-resolution gridded products [29].

B. L2G Compositing Approach

Conventionally, different orbits of data are geometrically corrected prior to compositing. The gridding process will

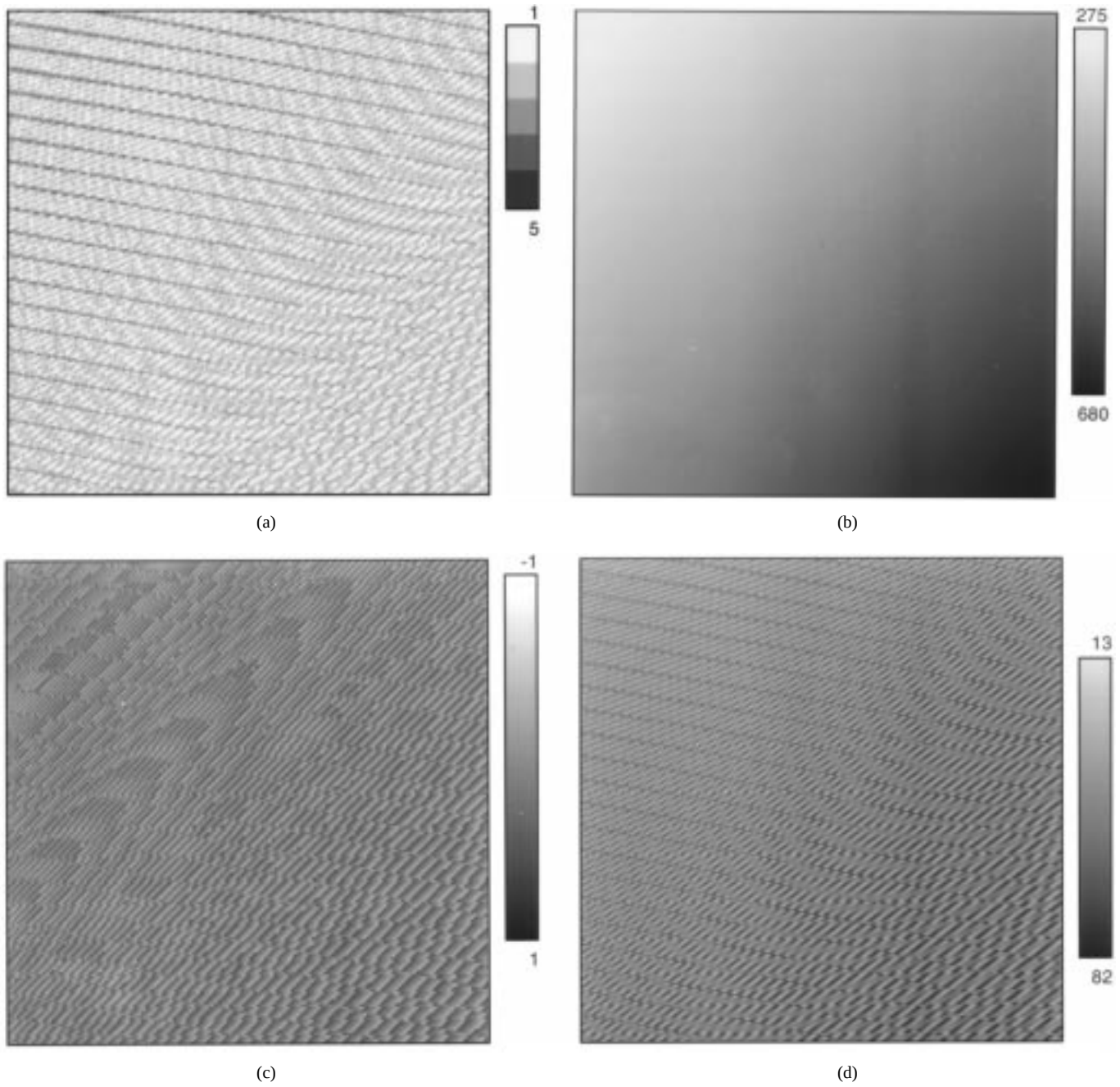

Fig. 10. L2G midlatitude example of a single granule of simulated MODIS data sensed over the Chesapeake Bay, MD. A region of 256 × 256 1-km grid cells is shown, corresponding to approximately 2 × 2° and defined in the Integerized Sinusoidal projection, illustrating: (a) the number of observations, (b) the observation sample number for layer one, (c) the $\Delta sample$ for layer one, and (d) the *obscov* value of the observation stored in layer one. Multiple observations of the same grid cell are ranked and stored in layers according to the *obscov* value (the observation/grid cell intersection area divided by the area of the observation footprint), with layer one containing the observation with the highest *obscov* value at that grid cell.

change the geometric and/or radiometric structure of the gridded observations and may discard potentially useful observations. The L2G structure allows the compositing procedure to select or combine original ungridded observations, avoiding some of these problems.

Fig. 9 illustrates how MODIS compositing is performed by reading the daily L2G tiles for each of the input parameters required by the Level 3 compositing process. Only those observations most relevant to the compositing process within each grid cell are selected for inclusion in the composite. For example, observations sensed far from nadir, with different atmospheric and cloud conditions, or with poor geolocation and poor geophysical parameter quality may be removed by examination of the corresponding L2G sensing geometry and geophysical parameter data.

VII. L2G Storage Examples

The L2G algorithm has been implemented as part of the MODIS production software. For illustrative purposes, the software was run on simulated MODIS data for a midlatitude,

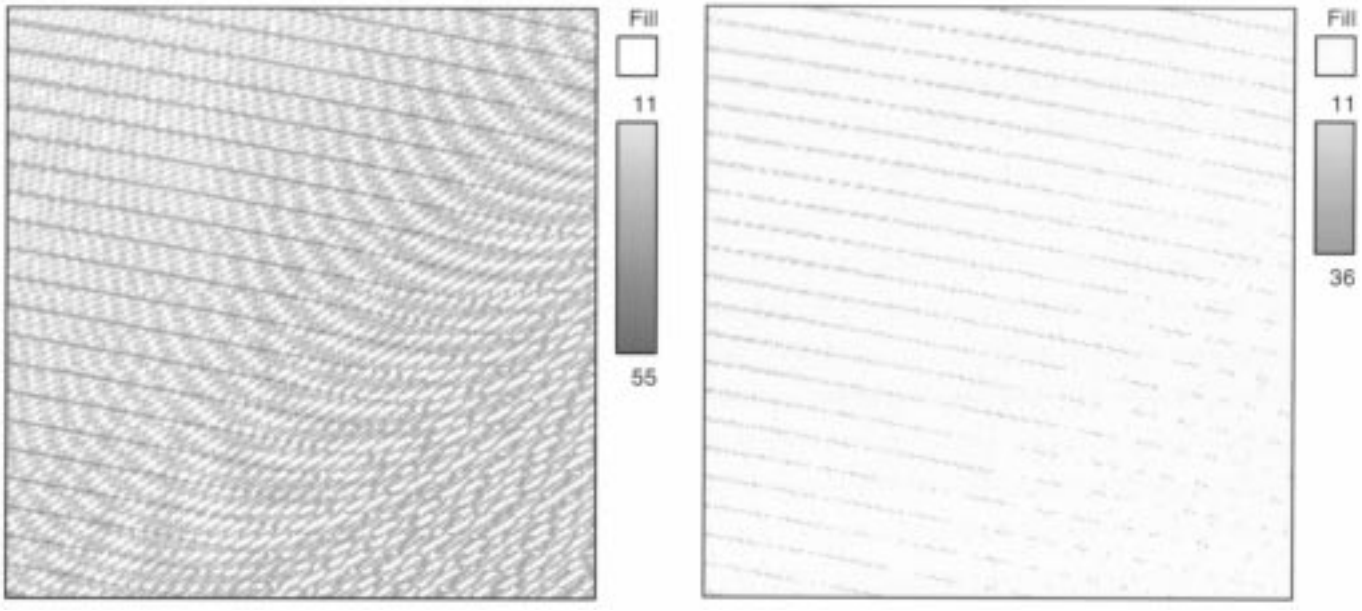

(e) (f)

Fig. 10. (*Continued.*) L2G midlatitude example of a single granule of simulated MODIS data sensed over the Chesapeake Bay, MD. A region of 256 × 256 1-km grid cells is shown corresponding to approximately 2 × 2° and defined in the Integerized Sinusoidal projection, illustrating: (e) the *obscov* value of the observation stored in layer two and (f) the *obscov* value of the observation stored in layer three. Multiple observations of the same grid cell are ranked and stored in layers according to the *obscov* value (the observation/grid cell intersection area divided by the area of the observation footprint), with layer one containing the observation with the highest *obscov* value at that grid cell.

single granule case and for a polar, multiple granule case. In both cases, a *cellcov* threshold of 24% was used.

A. Midlatitude, Single Granule Example

Fig. 10 shows elements of the L2G structure for simulated 1-km observations sensed by a single granule over the Chesapeake Bay, lying close to Washington DC. A region of 256 × 256 1-km grid cells corresponding to approximately 2 × 2° and defined in the Integerized Sinusoidal projection is shown. The data were stored so that for each grid cell, the observation with the maximum *obscov* value was stored in layer one and the observations with progressively smaller *obscov* values were stored in layers two, three, four, etc. Fig. 10 shows (a) the number of observations per grid cell, (b) the observation sample numbers for *obscov* layer one, (c) the $\Delta sample$ for *obscov* layer one, and (d)–(f) the *obscov* values for layers one to three, respectively.

The number of observations per grid cell vary from one to five, with a mean of 1.73 over the region shown in Fig. 10(a). Up to four observations are expected per grid cell using a *cellcov* threshold of 24%. However, the observations occur toward the edge of the granule where they overlap in consecutive scans, giving up to five observations per grid cell. The scan overlap regions appear as dark near-horizontal lines that decrease in thickness toward nadir (sample 677) and show the scanning orientation. The observation sample numbers in Fig. 10(b) illustrate this, showing increasing sample numbers from the west edge (sample 275) to the east edge (sample 680) of the region.

The $\Delta sample$ data shown in Fig. 10(c) have a sawtooth pattern with values varying over a $+1$--1 range. The frequency of the sawtooth pattern is of the order of three grid cells per cycle at the north of the region and ten grid cells per cycle in the southeast corner of the region. This pattern reflects the change in the subpixel location of the observation centers relative to the regular grid cell locations. A strong moiré pattern is observed in parts of Fig. 10 and in Fig. 11. This is produced by a beat pattern that arises if an image contains periodicities that are close to half the display sampling frequency.

The *obscov* layers shown in Fig. 10(d)–(f) contain two patterns, a combination of the scan overlap seen in Fig. 10(a) and the sawtooth pattern seen in Fig. 10(c). Most of the granule observations are stored in layers one and two, with fewer observations stored in layer three. Layer three contains observations that occur primarily in the scan overlap region. Layers four and five are not shown, as less than 1% of their grid cells contained observations. The mean *obscov* value is 44% in layer one, 25% in layer two, and 21% in layer three.

B. Polar Multiple Granule Example

Fig. 11 shows elements of the L2G structure for two overlapping, simulated granules sensed on the same day at 72° N. A region of 256 × 256 500-m grid cells is shown, corresponding to approximately 1 × 1°, defined in the Lambert Azimuthal Equal-Area projection. The observations were simulated as being sensed at 500-m resolution. Fig. 11 shows (a) the number of observations per grid cell, (b) the sample number, and (c) *obscov* values for layer one (the layer storing for each grid cell the observation with the maximum *obscov* value).

The two sets of lines seen in Fig. 11(a) show the different orientations of the two overlapping granules. One granule is seen by the narrow dark-gray lines running nearly diagonally

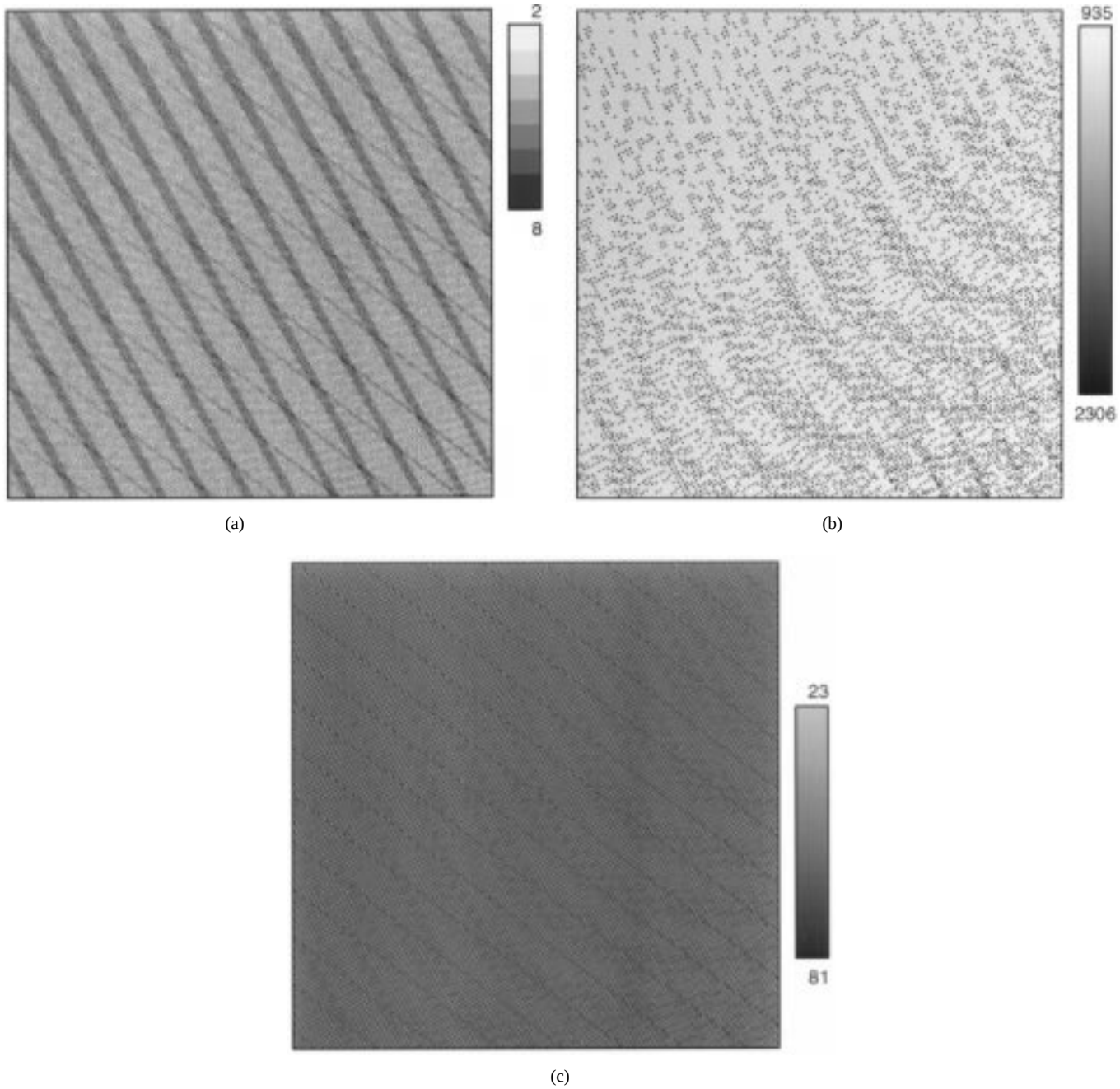

Fig. 11. L2G high-latitude example of two overlapping granules of simulated MODIS data sensed on the same day at 72° N. A region of 256 × 256 500-m grid cells is shown, corresponding to approximately 1 ×1° defined in the Lambert Azimuthal Equal-Area projection illustrating: (a) the number of observations, (b) the observation sample number for layer one, and (c) the *obscov* value of the observation stored in layer one. Multiple observations of the same grid cell are ranked and stored in layers according to the *obscov* value (the observation/grid cell intersection area divided by the area of the observation footprint), with layer one containing the observation with the highest *obscov* value at that grid cell.

across the region, and the other is seen by the more vertical lines. The lines correspond to the regions of scan overlap within each granule. There are a maximum of eight observations per grid cell that occur where the overlap regions of the two granules intersect. The mean number of observations is 3.6, roughly twice the number in the single granule example, as expected.

The sample number data shown in Fig. 11(b) provide a good indication of which granule each of the observations stored in *obscov* layer one came from. The sample numbers from one granule vary near nadir (sample number 1354) from 935 to 1270 and are displayed as light points, while the sample numbers of the other granule vary from 2098 to 2306 and are displayed as darker points.

Fig. 11(c) shows the *obscov* values for the first layer. These data have less-pronounced striping and moiré patterns and a higher mean *obscov* value of 55% than the single granule data shown in Fig. 10(d). This illustrates that, where MODIS orbits overlap more frequently, the likelihood of obtaining a representative sample of an output Level 3 grid cell will increase.

VIII. Planned Near-Term Improvements

There are several areas where future work is needed on the L2G approach: a more complete observation model, determining the optimum criteria for keeping observations, faster algorithms, and detailed comparisons of new algorithms with heritage algorithms.

The MODIS observation footprint model will be enhanced to take into account the proper along-scan nesting of the higher resolution 250- and 500-m bands within the coarser 1-km bands. Higher order approximations of the system PSF are required to model the atmospheric PSF and instrument characteristics, such as optical blur. The effects of terrain on the 500- and 250-m observations will be investigated once suitable global terrain models are available at 500- and 250-m spatial resolutions. The sensitivity of the L2G approach, with respect to MODIS geolocation errors, will be investigated using the improved observation model.

The methodology for reducing the number of observations stored per grid cell will be examined, with respect to the results of post-MODIS launch geolocation characterization activities. Since the L2G algorithm was developed primarily for MODIS land applications, optically thick cloud pixels are not of interest. Consequently, computing and data storage resources may be saved by eliminating cloudy pixels prior to generation of L2G products. This may provide approximately a 50% saving, as it is conservatively estimated that approximately 50% of the globe is cloud covered at any one time [30]. However, until the MODIS cloud screening algorithms are mature, cloudy pixels will be kept in the L2G products.

IX. Conclusion

The methodology used to store a number of the MODIS land data products and enable their efficient processing and reprocessing has been described. The methodology, termed L2G, has several advantages over conventional approaches used to store global coverage remotely sensed data sets. It requires that the remotely sensed observations are geolocated to subpixel accuracy, and it stores the subpixel location and the relative intersection area of the observations falling over each output grid cell over a 24-h period. These information will enable existing terrestrial remote-sensing algorithms to be more robustly and accurately implemented and may aid the development of new algorithms that exploit multiple observations of the surface. The MODIS land gridding and compositing approach that uses this information is described to illustrate these points. MODIS land data products and the Level 2 grid software used to produce them will be made available to the public as part of the EOS data and software distribution policy. Other instruments and disciplines may find this a useful tool to fully exploit satellite data, especially instruments that observe the surface over a range of viewing geometries, e.g., Across Track Scanning Radiometer (ATSR) [31], [32] and MISR [33].

Acknowledgment

The authors thank C. Justice and the anonymous reviewers for their comments and suggestions. They also thank V. Kalb, Y. Tung and K. Yang for their contributions to the Level 2 grid code development.

References

[1] V. V. Solomonson, W. L. Barnes, P. W. Maymon, H. E. Montgomery, and H. Ostrow, "MODIS: Advanced facility instrument for studies of the earth as a system," *IEEE Trans. Geosci. Remote Sensing*, vol. 27, pp. 145–153, Jan. 1989.

[2] S. W. Running, C. O. Justice, V. V. Salomonson, D. Hall, J. Barker, Y. J. Kaufmann, A. H. Strahler, A. R. Huete, J.-P. Muller, V. Vanderbilt, Z. M. Wan, P. Teillet, and D. Carneggie, "Terrestrial remote sensing science and algorithms planned for EOS/MODIS," *Int. J. Remote Sensing*, vol. 15, pp. 3587–3620, 1994.

[3] C. O. Justice, E. Vermote, J. R. G. Townshend, R. Defries, D. P. Roy, D. K. Hall, V. V. Salomonson, J. L. Privette, G. Riggs, A. Strahler, W. Lucht, R. B. Myneni, Y. Knjazihhin, S. W. Running, R. R. Nemani, Z. Wan, A. R. Huete, W. van Leeuwen, R. E. Wolfe, L. Giglio, J.-P. Muller, P. Lewis, and M. J. Barnsley, "The Moderate Resolution Imaging Spectroradiometer (MODIS): Land remote sensing for global change research," this issue, pp. 1228–1249.

[4] B. N. Holben, "Characteristics of maximum-value composite images from temporal AVHRR data," *Int. J. Remote Sensing*, vol. 7, pp. 1417–1434, 1986.

[5] R. A. Schowengerdt, *Remote Sensing Models and Methods for Image Processing*. San Diego, CA: Academic, 1997.

[6] G. Konecny, "Methods and possibilities for digital differential rectification," *Photogramm. Eng. Remote Sensing*, vol. 45, no. 6, pp. 727–734, 1979.

[7] K. R. Castleman, *Digital Image Processing*. Englewood Cliffs, NJ: Prentice-Hall, 1979.

[8] S. Shlien, "Geometric correction, registration, and resampling of Landsat imagery," *Can. J. Remote Sensing*, vol. 5, pp. 74–89, 1979.

[9] R. G. Keys, "Cubic convolution interpolation for digital image processing," *IEEE Trans. Acoust., Speech, Signal Processing*, vol. ASSP-29, pp. 1153–160, 1981.

[10] S. K. Park and R. A. Schowengerdt, "Image reconstruction by parametric cubic convolution," *Comput. Vision, Graph. Image Processing*, vol. 23, pp. 258–272, 1983.

[11] B. Khan, L. W. B. Hayes, and A. P. Cracknell, "The effects of higher-order resampling on AVHRR data," *Int. J. Remote Sensing*, vol. 16, pp. 147–163, 1995.

[12] L. Breaker, "Estimating and removing sensor-induced correlation from advanced very high resolution radiometer satellite data," *J. Geophys. Res.*, vol. 95, pp. 9701–9711, 1990.

[13] R. E. Wolfe, J. C. Storey, E. Masuoka, and A. J. Fleig, "MODIS level 1A earth location algorithm theoretical basis document," in *NASA Tech. Memo. 104 594*, vol. 5. Greenbelt, MD: Goddard Space Flight Center, Apr. 1995.

[14] J. F. Moreno and J. Melia, "An optimum interpolation method applied to the resampling of NOAA AVHRR data," *IEEE Trans. Geosci. Remote Sensing*, vol. 32, pp. 131–151, Jan. 1994.

[15] S. E. Reichenbach, D. E. Koehler, and D. W. Strelow, "Restoration and reconstruction of AVHRR images," *IEEE Trans. Geosci. Remote Sensing*, vol. 33, pp. 997–1007, July 1995.

[16] B. J. Choudhury, N. E. Digirolamo, and T. J. Dorman, "A comparison of reflectances and vegetation indices from three methods of compositing the AVHRR-GAC data over Northern Africa," *Remote Sens. Rev.*, vol. 10, pp. 245–263, 1994.

[17] J. Cihlar, D. Manak, and M. D'Iorio, "Evaluation of compositing algorithms for AVHRR data over land," *IEEE Trans. Geosci. Remote Sensing*, vol. 32, pp. 427–437, Mar. 1994.

[18] D. P. Roy, "Investigation of the maximum normalized difference vegetation index (NDVI) and the maximum surface temperature (Ts) AVHRR compositing procedures for the extraction of NDVI and Ts over forest," *Int. J. Remote Sensing*, vol. 18, pp. 2383–2401, 1997.

[19] D. M. Stoms, M. J. Bueno, and F. W. David, "Viewing geometry of AVHRR image composites derived using multiple criteria," *Photogramm. Eng. Remote Sensing*, vol. 63, pp. 681–689, 1997.

[20] D. Meyer, M. M. Verstraete, and B. Pinty, "The effect of surface anisotropy and viewing geometry on the estimation of NDVI from AVHRR," *Remote Sens. Rev.*, vol. 12, pp. 3–27, 1995.

[21] W. van Leeuwen, A. R. Heuete, S. Jia, and C. L. Walthall, "Comparison of vegetation index compositing scenarios: BRDF versus maximum VI approaches," in *Proc. 1996 Int. Geosci. Remote Sensing Symp.*, Lincoln, NE, pp. 1423–1425.

[22] J. R. G. Townshend, C. O. Justice, C. Gurney, and J. McManus, "The impact of misregistration on change detection," *IEEE Trans. Geosci. Remote Sensing*, vol. 30, pp. 1054–1060, Sept. 1992.
[23] Jet Propulsion Laboratory, "DEM auxiliary datasets preparation plan: digital elevation mapping support to the EOS/AM-1 platform," Jet Propul. Lab., California Inst. Technol., Pasadena, JPL D-13508, Release 2, 1997.
[24] U.S. Department of Defense, Defense Mapping Agency (DMA) Technical Report (TR) DMATR 8350.2: Department of Defense World Geodetic System 1984—Its Definition and Relationship with Local Geodetic Systems, National Imagery and Mapping Agency, Combat Support Center, ATTN: PMSR, STD-17, 6001 MacArthur Boulevard, Bethesda, MD 20816-5001, 1994.
[25] A. J. Fleig, P. A. Hubanks, J. C. Storey, and R. E. Wolfe, "Geolocation of data from the earth observing system's MODIS instrument: An analysis of location accuracy," in *Proc. IGARSS'95*, Florence, Italy, pp. 129–131.
[26] J. P. Snyder, *Map Projections—A Working Manual*, Washington, DC, United States Government Printing Office, U.S. Geological Survey Professional Paper 1395, 1987.
[27] F. P. Preparata and M. I. Shamos, *Computational Geometry: An Introduction*. New York, Springer-Verlag, 1988.
[28] D. P. Roy, B. Devereux, B. Grainger, and S. White, "Parametric geometric correction of airborne thematic mapper imagery," *Int. J. Remote Sensing*, vol. 18, pp. 1865–1887, 1997.
[29] D. G. Baldwin, W. J. Emery, and P. B. Cheeseman, "Higher resolution earth surface features from repeat moderate resolution satellite imagery," *IEEE Trans. Geosci. Remote Sensing*, vol. 36, pp. 244–255, Jan. 1998.
[30] I. I. Mokhov and M. E. Schlesinger, "Analysis of global cloudiness 2. Comparisons of ground-based and satellite-based cloud climatologies," *J. Geophys. Res.*, vol. 99, pp. 17 045–17 065, 1994.
[31] C. Godsalve, "Bidirectional reflectance sampling by ATSR-2—A combined orbit and scan model," *Int. J. Remote Sensing*, vol. 16, pp. 269–303, 1995.
[32] A. J. Prata, R. P. Cechet, I. J. Barton, and D. T. Llewellyn Jones, "The Along Track Scanning Radiometer for ERS-1: Scan geometry and data simulation," *IEEE Trans. Geosci. Remote Sensing*, vol. 28, pp. 3–123, Jan. 1990.
[33] D. J. Diner, C. J. Bruegge, J. V. Martonchik, T. P. Ackerman, R. Davies, S. A. W. Gerstl, H. R. Gordon, P. J. Sellers, J. Clark, J. A. Daniels, E. D. Danielson, V. G. Duval, K. P. Klassen, G. W. Lilienthal, D. I. Nakamoto, R. Pagano, and T. H. Reilly, "MISR: A Multi-angle Imaging SpectroRadiometer for geophysical and climatological research from EOS," *IEEE Trans. Geosci. Remote Sensing*, vol. 27, pp. 200–214, Mar. 1989.

Robert E. Wolfe received the B.Sc. degree in mathematics and physics from Bridgewater College, Bridgewater, VA, in 1980.

He is currently a Chief Scientist with Raytheon STX working at NASA's Goddard Space Flight Center, Greenbelt, MD. He is working with the MODIS Science Team and coordinates MODIS geolocation and Level 3 land product generation. Before joining MODIS, he spent over ten years building processing systems for high-resolution imagery sensed by the Landsat TM and SPOT sensors. His research interests include satellite image geolocation, elevation model generation, and the production of terrestrial geophysical parameters from satellite data.

David P. Roy, for a photograph and biography, see this issue, P. 1248.

Eric Vermote (M'95), for a photograph and biography, see this issue, p. 1248.